







RESEARCH ARTICLE | JULY 10 2025

## Optical properties of Zr-doped AlN epilayers

H. Alwan ; M. Almohammad ; J. Li ; J. Y. Lin ; H. X. Jiang  



*APL Mater.* 13, 071115 (2025)

<https://doi.org/10.1063/5.0277907>

 CHORUS





**Your One-Stop Shop for the  
Best Brands in Optics**

- Extensive inventory with over 34,000 products available & 2,900 new products
- Fast shipping from our 9 distribution centres around the globe
- Bringing 80+ years of optical expertise to customers worldwide

**eo Edmund**  
optics | worldwide

[Shop Now](#)

# Optical properties of Zr-doped AlN epilayers

Cite as: APL Mater. 13, 071115 (2025); doi: 10.1063/5.0277907

Submitted: 26 April 2025 • Accepted: 29 June 2025 •

Published Online: 10 July 2025



H. Alwan,<sup>1</sup> M. Almohammad,<sup>1</sup> J. Li,<sup>1</sup> J. Y. Lin,<sup>1</sup> and H. X. Jiang<sup>a)</sup>

## AFFILIATIONS

Department of Electrical and Computer Engineering, Texas Tech University, Lubbock, Texas 79409, USA

<sup>a)</sup> Author to whom correspondence should be addressed: [hx.jiang@ttu.edu](mailto:hx.jiang@ttu.edu)

## ABSTRACT

Aluminum nitride (AlN) doped with zirconium (Zr), AlN:Zr, an ultrawide bandgap semiconductor, has been theoretically predicted as a promising material for quantum information systems, piezoelectric applications, and photoconductive semiconductor switches. We report on the optical characterization of AlN:Zr epilayers synthesized by metal-organic chemical vapor deposition. Photoluminescence measurements demonstrate that Zr doping introduces distinct emission features near 1.8, 2.46, and 3.63 eV. These emission lines, together with a prominent absorption peak centered at 1.78 eV whose intensity increases with Zr content, are identified as originating from the complex between Zr and nitrogen vacancy,  $Zr_{Al}-V_N$ . Evidence indicates that the dominant optical absorption and emission pathways involve the neutral charge state of this complex,  $(Zr_{Al}-V_N)^0$ . This finding is highly encouraging, given that  $(Zr_{Al}-V_N)^0$  is considered an ideal candidate for a qubit. Concurrently, our analysis reveals that Zr incorporation also promotes the formation of deleterious aluminum vacancy ( $V_{Al}$ ) and  $V_{Al}$ -complex related defects, necessitating process optimization to minimize their concentration for practical device realization.

© 2025 Author(s). All article content, except where otherwise noted, is licensed under a Creative Commons Attribution-NonCommercial 4.0 International (CC BY-NC) license (<https://creativecommons.org/licenses/by-nc/4.0/>). <https://doi.org/10.1063/5.0277907>

Aluminum nitride (AlN) is an ultrawide bandgap ( $E_g \approx 6.1$  eV, direct) semiconductor<sup>1</sup> with significant technological importance, particularly in deep UV (DUV) optoelectronics.<sup>1–6</sup> Its robust physical properties, notably a high critical breakdown field ( $\sim 15$  MV/cm),<sup>7</sup> excellent thermal conductivity ( $\sim 320$  W·m<sup>−1</sup> K<sup>−1</sup>),<sup>8–10</sup> substantial electron mobility,<sup>11</sup> and inherent chemical and thermal stability, also position it as a prime candidate material for high-power and high-temperature electronic devices.<sup>12–17</sup> Beyond these established applications, AlN doped with zirconium (Zr), AlN:Zr, has recently garnered attention as a promising platform for quantum information technologies. This interest stems from the prediction that Zr readily substitutes onto the Al sublattice ( $Zr_{Al}$ ), introducing a donor state  $\sim 1.4$  eV below the conduction band minimum (CBM).<sup>18</sup> Moreover, the neutral defect complex comprising ( $Zr_{Al}$ ) and an adjacent nitrogen vacancy ( $V_N$ ), denoted by  $(Zr_{Al}-V_N)^0$ , is theoretically predicted to host unique spin states suitable for quantum manipulation. Crucially, these quantum states are expected to exhibit reduced coupling to conduction band states compared to simpler donors, potentially offering enhanced coherence times similar to the well-known  $NV^-$  center in diamond.<sup>18</sup> As ( $Zr_{Al}$ ) and  $(Zr_{Al}-V_N)$  donor levels are sufficiently deep to support extremely low leakage currents, AlN:Zr also possesses all the necessary properties as an ideal candidate material for photoconductive

semiconductor switches (PCSS) to support high-voltage and high-power operations.

Inspired by the theoretical prediction, Zr doped AlN films have been investigated by several groups.<sup>19–21</sup> To incorporate Zr into AlN, previous Zr doped AlN thin film materials were prepared by reactive magnetron sputtering and ion implantation.<sup>19–21</sup> However, these materials suffer from inferior crystalline quality as reflected by the broad full width at half-maximum (FWHM) of x-ray diffraction (XRD) rocking curves of the AlN (002) planes exceeding  $1.4^\circ$ .<sup>19–21</sup> Ion implantation and reactive magnetron sputtering processes tend to introduce defects and damage to the target material, which can have adverse effects on the experimental results, limiting the understanding of the impact of Zr incorporation in AlN on the optical and spin properties.

More recently, we reported the synthesis of Zr doped AlN (AlN:Zr) epilayers by metal organic chemical vapor deposition (MOCVD).<sup>22</sup> Secondary ion mass spectrometry (SIMS) characterization revealed a uniform Zr concentration, whereas x-ray photoelectron spectroscopy (XPS) studies confirmed that Zr substitutes on the Al site ( $Zr_{Al}$ ), corroborating with the theoretical prediction.<sup>22</sup> For films with a thickness of 1.8  $\mu$ m, XRD characterization results revealed that AlN:Zr epilayers retain high crystalline quality for high Zr doping levels.<sup>22</sup> We report here on the investigation of the

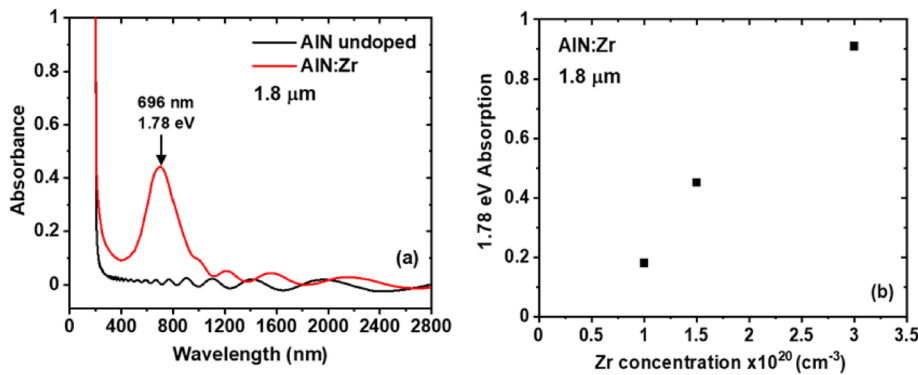


**FIG. 1.** (a) Optical absorption spectra of representative undoped and Zr-doped AlN (AlN:Zr) epilayers. (b) Zr concentration dependence of absorption at 1.78 eV in AlN:Zr epilayers.

optical properties of AlN:Zr epilayers via photoluminescence (PL) and optical absorption spectroscopy. With the guidance provided by previous theoretical studies,<sup>18,23</sup> we aim to identify major impurities and defects related to Zr doping. We believe that the present results set the stage for the experimental investigation of spin properties as well as many other possible applications of the AlN:Zr material system.

Undoped and Zr doped AlN epilayers are grown using MOCVD on 2-in. c-plane sapphire substrates. Trimethylaluminum (TMA) and ammonia ( $\text{NH}_3$ ) were utilized as the Al and N precursors, respectively, whereas the Zr precursor of tetrakis(dimethylamino) zirconium [TDMAZr] was supplied to the reactor using  $\text{H}_2$  as a carrier gas. An AlN buffer layer of 20 nm was first deposited at  $750^\circ\text{C}$ , followed by the growth of a Zr doped AlN epilayer of 1.8  $\mu\text{m}$  in thickness at  $1250^\circ\text{C}$ . Two different PL spectroscopy systems were used to characterize the PL properties of AlN:Zr epilayers. The first system consists of a 20 ns excimer laser ( $\lambda_{\text{exc}} = 193 \text{ nm}$ , 6.42 eV) operating at a repetition rate of 40 Hz with an average optical power of 4 W and an optical fiber coupled spectrometer. The second system consists of a frequency-quadrupled femtosecond (fs) Ti:sapphire laser ( $\lambda_{\text{exc}} = 195 \text{ nm}$ , 6.35 eV) operating at 76 MHz with an average optical power of 1 mW and a 1.3 m monochromator in conjunction with a micro-channel plate photomultiplier tube (MCP-PMT). To account for the fact that the band edge emission in AlN is with a polarization of  $E \parallel c$ ,<sup>1,2</sup> the PL emission was collected at an angle of about  $45^\circ$  with respect to the c-axis. Optical absorption spectra of undoped and Zr doped AlN epilayers were measured using an Agilent Cary 5000 UV-Vis-NIR spectrophotometer. SIMS measurements were performed (by Charles Evans & Associates) to determine Zr doping concentration, [Zr]. The Zr concentrations were also routinely measured using the XPS technique (Physical Electronics PHI 5000 Versa Probe II Hybrid), and the measurement results correlate well with those of SIMS. Before surveying scans of XPS measurements, the surface was etched with an argon (Ar) ion gun to remove any dust and surface adsorbents.

Optical absorption spectra for representative undoped AlN and AlN:Zr epilayers are displayed in Fig. 1(a). In addition to the sharp band edge absorption peak near 200 nm, Zr doping induces an optical absorption peak at around 696 nm (1.78 eV) in the AlN:Zr sample, which indicates that Zr doping has introduced a new energy level in AlN:Zr, consistent with our previously reported

results.<sup>22</sup> The absorption strength increases continuously with Zr concentration, as shown in Fig. 1(b), reinforcing that this absorption line is due to the presence of Zr in AlN. For the sample with a Zr concentration of  $[\text{N}_{\text{Zr}}] = 3 \times 10^{20} \text{ cm}^{-3}$ , determined by SIMS and

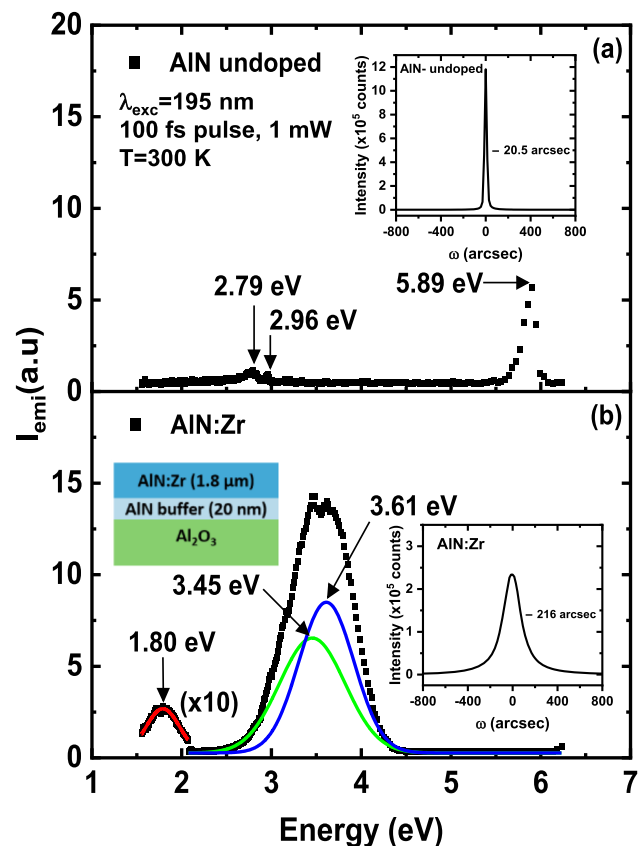


**FIG. 2.** Room temperature ( $T = 300 \text{ K}$ ) PL spectra and XRD (002) rocking curves for representative (a) undoped AlN and (b) AlN:Zr epilayers, excited by a fs laser ( $\lambda_{\text{exc}} = 195 \text{ nm}$ ) with an average power of 1 mW. The schematic layer structure of the AlN:Zr epilayer is also shown as the inset in (b). Marked spectral peak positions are obtained by fitting using Gaussian functions.

XPS measurements, the measured optical absorption at 1.78 eV is 90%.

Figure 2 compares the room temperature PL emission spectra of representative (a) undoped AlN and (b) AlN:Zr epilayers excited by the 1 mW fs laser ( $\lambda_{\text{exc}} = 195$  nm). The undoped AlN epilayer predominantly exhibits the band edge transition at 5.89 eV. Two emission bands appearing at about 2.79 and 2.96 eV related to isolated Al vacancy ( $V_{\text{Al}}$ ) defects<sup>23–25</sup> are also visible with much lower emission intensities. The results are indicative of high crystalline quality and purity of undoped AlN. This is corroborated by the narrow FWHM of (002) XRD rocking curve of only 20.5 arc sec shown in the inset of Fig. 2(a).

In comparison, the band edge emission line is absent, and the most dominant emission lines in the AlN:Zr epilayer with its layer structure shown in the inset of Fig. 2(b) are at 3.45 and 3.61 eV. The incorporation of Zr also reduced the crystalline quality of AlN as manifested by the increase in the FWHM of the (002) XRD rocking curve to 216 arc sec for AlN:Zr with  $[N_{\text{Zr}}] = 1 \times 10^{20} \text{ cm}^{-3}$ . Notably, the emission line around 3.45 eV was previously reported for undoped and Si doped AlN epilayers, with its origin ascribed to the  $V_{\text{Al}}$ -complex recombination centers.<sup>23–25</sup> In AlN, it is well known that  $V_{\text{Al}}$ -complexes with  $-1$  to  $-3$  charge states are the principal electron traps, and minimizing their presence is critical for achieving  $n$ -type AlN by Si doping.<sup>23–29</sup> Comparing the PL results shown in Figs. 2(a) and 2(b), the incorporation of Zr appears to significantly enhance the generation of  $V_{\text{Al}}$  related defects due to Zr-doping induced Fermi level shifting toward the CBM and reduction in the formation energies of  $V_{\text{Al}}$  related defects.<sup>23</sup> Based on the XPS measurement results, we indeed noted that AlN:Zr epilayers contain a slightly higher V/III ratio than undoped AlN epilayers. On the other hand, the emission line at 3.61 eV has not been previously observed in AlN epilayers and is presumably introduced by Zr doping. The FWHMs of the 3.45 and 3.61 eV peaks are 0.85 and 0.72 eV, respectively. Zr doping also introduced another weak emission line near 1.8 eV.

The PL spectrum of AlN:Zr excited by the 1 mW fs laser ( $\lambda_{\text{exc}} = 195$  nm) has also been measured at 10 K, and the results are shown in Fig. 3. Emission peaks associated with  $V_{\text{Al}}$ -complex recombination centers of different charge states are dominant and become resolvable at low temperatures. The 3.61 eV peak related to the presence of Zr is blue shifted to 3.74 eV at 10 K. It is interesting to note that the Zr related emission line at 1.8 eV is red shifted to 1.67 eV at 10 K, and the observed spectral shift corresponds well with the longitudinal optical (LO) phonon energy in AlN of  $\sim 110$  meV.<sup>30</sup>

Figure 4 compares the room temperature PL emission spectra of representative (a) undoped AlN and (b) AlN:Zr epilayers under a 4 W excimer laser ( $\lambda_{\text{exc}} = 193$  nm) excitation, showing that undoped AlN exhibits only a band edge emission line at 5.9 eV and the two defect emission lines at 2.79 and 2.96 eV seen in Fig. 2(a) are absent. This is likely due to the effect of impurity concentration saturation under high power excitation. For AlN:Zr samples under excimer laser excitation, the Zr-doping induced emission line appears at 3.63 eV and becomes the most dominant, indicating that the concentration of Zr related defects is higher than that of  $V_{\text{Al}}$ -complexes. The PL spectrum shown in Fig. 4(b) also reveals a weaker peak at 2.46 eV, which has not been observed previously and is presumably related to Zr. The band edge transition line near 5.9 eV also becomes observable under strong excitation by the excimer laser.

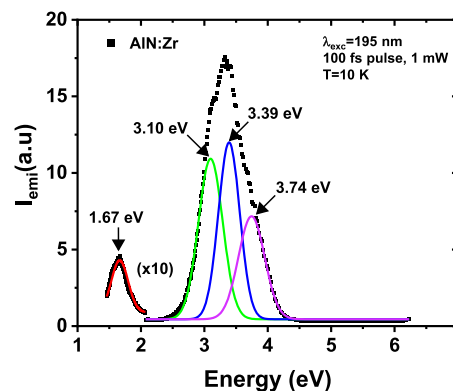


FIG. 3. Low temperature ( $T = 10$  K) PL spectra of AlN:Zr epilayers excited by a fs laser ( $\lambda_{\text{exc}} = 195$  nm) with an average power of 1 mW. Marked spectral peak positions are obtained by fitting using Gaussian functions.

We noted that the weak 1.8 eV emission line seen in Fig. 2(b) is absent in Fig. 4(b). Other than the substantial difference in the average excitation power between the two excitation laser sources, their pulse widths and repetition rates are also hugely different. Due to the low repetition rate (40 Hz) as well as the long pulse width (20 ns) of the excimer laser, emission lines with ultrafast recombination processes are more difficult to capture. Comparing the results between Figs. 2(a) and 2(b) as well as between Figs. 4(a) and 4(b), we can conclude that Zr doping strongly influenced the electronic structure of AlN and introduced distinct emission peaks at 1.8, 2.46, and 3.63 eV, while the physical origin of the 1.8 eV emission appears different from those of 2.46 and 3.63 eV, as it is absent under excitation by the

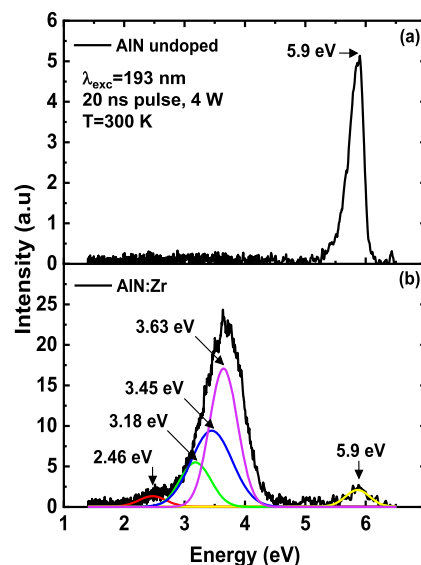


FIG. 4. Room temperature ( $T = 300$  K) PL spectra of representative (a) undoped and (b) AlN:Zr epilayers excited by an excimer laser ( $\lambda_{\text{exc}} = 193$  nm) with an average power of 4 W. Marked spectral peak positions in (b) are obtained by fitting using Gaussian functions.

excimer laser with a longer pulse width (20 ns) and slower repetition rate (40 Hz).

Based on a previous theoretical insight,  $Zr_{Al}$  donors can assume +1, 0, and -1 charge states with a predicted energy level of about 1.4 eV below the CBM for the neutral charge state,  $(Zr_{Al})^0$ .<sup>18</sup> On the other hand, the complex between Zr and nitrogen vacancy can also assume +1, 0, and -1 charge states. When in the neutral charge state,  $(Zr_{Al}-V_N)^0$  complexes are stable in the  $S = 1$  state and from 2.58 to 1.59 eV below the CBM and possess the desired properties of solid-state qubits.<sup>18</sup> Although the -1 charge state of the complex  $(Zr_{Al}-V_N)^{-1}$  favors a low-spin  $S = 1/2$  configuration, uninteresting as a qubit candidate, it can participate in the optical transitions in AlN:Zr. Therefore, two different groups of optical transition lines in AlN:Zr are expected. The first group involves transitions between a band and Zr-related defects, and the second group involves the spin conserving internal (intradefect) transitions.

The predicted optical absorption between  $(Zr_{Al}-V_N)^0$  and the conduction band occurs at 3.07 eV, described by the process of  $(Zr_{Al}-V_N)^0 + hv (3.07 \text{ eV}) \rightarrow (Zr_{Al}-V_N)^+ + e^-$ .<sup>18</sup> However, the absorption spectrum shown in Fig. 1(a) exhibits no visible peak near 3.07 eV (404 nm). Since the calculated energy level of the -1 charge state of the complex between  $Zr_{Al}$  and  $V_N$ ,  $(Zr_{Al}-V_N)^{-1}$  is nearer the CBM than those of 2.58–1.59 eV for  $(Zr_{Al}-V_N)^0$ ,<sup>18</sup> we propose that the dominant optical absorption peak at 1.78 eV observed in Fig. 1 is due to the optical absorption process described by  $(Zr_{Al}-V_N)^- + hv (1.78 \text{ eV}) \rightarrow (Zr_{Al}-V_N)^0 + e^-$ . This scenario is plausible if the excitation cross section of  $(Zr_{Al}-V_N)^-$  is larger than that of  $(Zr_{Al}-V_N)^0$ . Regarding the spin conserving internal (intradefect) transition in  $(Zr_{Al}-V_N)^0$ , the calculation results predicted an optical absorption occurring at 2.83 eV (438 nm),<sup>18</sup> and an experimental measurement performed on Zr-implanted AlN yielded a possible absorption line at 2.6 eV,<sup>19</sup> which, however, cannot be resolved by the absorption spectrum shown in Fig. 1(a).

We now examine the observed optical emission lines under the above band-to-band excitation. The predicted optical emission line resulting from the recombination between electrons in the conduction band and the  $(Zr_{Al}-V_N)$  complex centers occurs at 2.11 eV,<sup>18</sup> which is reasonably close to the observed emission line near 2.46 eV seen in Fig. 4(b). With this understanding, we assign the observed emission line at 2.46 eV to the optical process of  $(Zr_{Al}-V_N)^+ + e^- \rightarrow (Zr_{Al}-V_N)^0 + hv (2.46 \text{ eV})$ . Conversely, the recombination process between  $(Zr_{Al}-V_N)^0$  and holes in the valence band described by  $(Zr_{Al}-V_N)^0 + h^+ \rightarrow (Zr_{Al}-V_N)^+ + hv (6.1\text{--}2.46 \text{ eV})$  is equally likely to occur, from which the emission peak energy is expected to be  $6.1\text{--}2.46 \text{ eV} = 3.64 \text{ eV}$ , which agrees with the observed value of

3.63 eV in Fig. 4(b) [and 3.61 eV in Fig. 2(b)]. In fact, the 3.63 eV emission line is the most dominant in AlN:Zr, implying that the concentration of  $(Zr_{Al}-V_N)^0$  is the highest among all defects present in AlN:Zr.

We attribute the 1.8 eV emission line observed in Fig. 2(b) to a spin-conserving internal transition within the  $(Zr_{Al}-V_N)^0$  defect in AlN. This assignment is supported by several key pieces of evidence. First, calculations previously predicted an emission line at 1.91 eV for this specific transition,<sup>18</sup> which is in reasonable agreement with the observed 1.8 eV. Second, the 1.8 eV emission is exclusively observed under fs laser excitation (76 MHz repetition rate, 1 mW power) and not with high-power excimer laser excitation (20 ns pulse width, 4 W, 40 Hz repetition rate). This suggests a distinct physical mechanism compared to typical band-to-impurity emissions. Third, the strong coupling of this 1.8 eV peak with phonons is characteristic of quantum defects. At 10 K, the peak position exhibits a red shift by an amount equal to the longitudinal optical (LO) phonon energy in AlN, as shown in Fig. 3. Finally, the spin-conserving internal transition was observed at 1.7 eV in ion-implanted AlN:Zr materials.<sup>19</sup> While these materials exhibit significantly poorer crystalline quality (indicated by a FWHM of the (002) XRD rocking curve exceeding  $1.5^\circ$ ), the presence of a similar transition further strengthens the assignment. Nevertheless, the exact mechanism of this emission line warrants further investigation. Techniques including time-resolved PL and correlation function measurements could add valuable insights.

Table I summarizes the PL peak positions and corresponding FWHM values observed in AlN:Zr at 300 K. Under excitation by the 195 nm fs laser, the 300 K PL spectrum exhibits three prominent emission peaks at 1.8, 3.45, and 3.61 eV with the corresponding linewidths of 0.44, 0.85, and 0.72 eV, respectively. Under excitation by the 193 nm ns excimer laser excitation, the 300 K spectrum resolved peaks at 2.46, 3.18, 3.45, 3.63, and 5.90 eV.

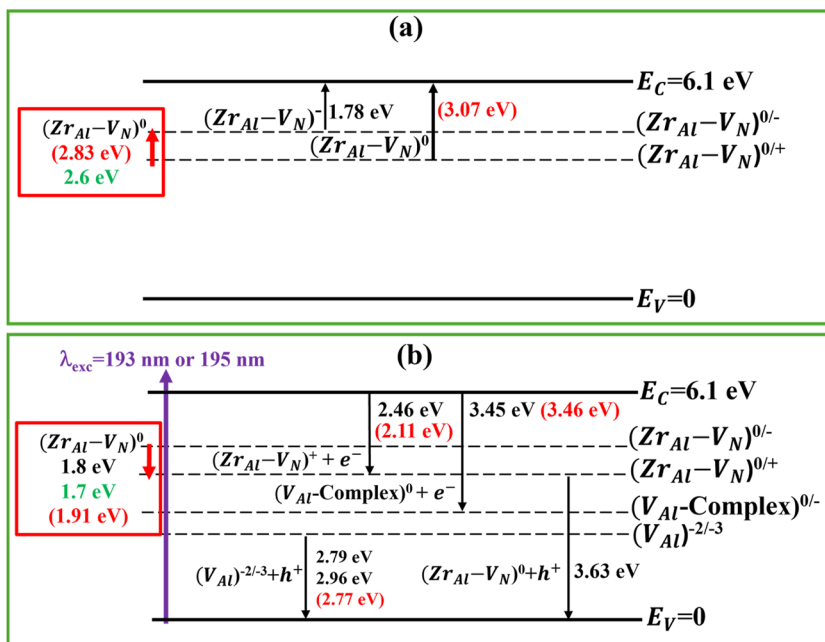
The emission line observed at 3.45 eV has been identified as due to the recombination between the electrons in the conduction band and  $(V_{Al}\text{-complex})^0$ , described by the process of  $(V_{Al}\text{-complex})^0 + e^- \rightarrow (V_{Al}\text{-complex})^- + hv (3.45 \text{ eV})$ .<sup>23</sup> The weak emission peak at 2.79 eV observed in undoped AlN has also been previously identified and is due to the recombination between isolated Al vacancies and holes in the valence band described by  $(V_{Al})^{-3} + h^+ \rightarrow (V_{Al})^{-2} + hv (2.79 \text{ eV})$ .<sup>23</sup>

Based on the PL results as well as the optical absorption data and prior calculation and experimental results,<sup>18,19,23</sup> we have constructed a plausible energy diagram illustrating the optical absorption and emission processes involving  $Zr_{Al}$  related defects in AlN:Zr. Figure 5(a) illustrates the optical absorption processes, while

**TABLE I.** Summary of PL peak positions and the corresponding FWHM observed in AlN:Zr measured under excitation by a fs laser ( $\lambda_{exc} = 195 \text{ nm}$ ) and by a ns excimer laser ( $\lambda_{exc} = 193 \text{ nm}$ ).

	$\lambda_{exc} = 195 \text{ nm}$ (fs pulse)							$\lambda_{exc} = 193 \text{ nm}$ (ns pulse)				
	300 K							300 K				
PL peak position (eV)	1.8	3.45	3.61	1.67	3.10	3.39	3.74	2.46	3.18	3.45	3.63	5.90
FWHM (eV)	0.44	0.85	0.72	0.31	0.45	0.39	0.48	0.53	0.60	0.87	0.55	0.47





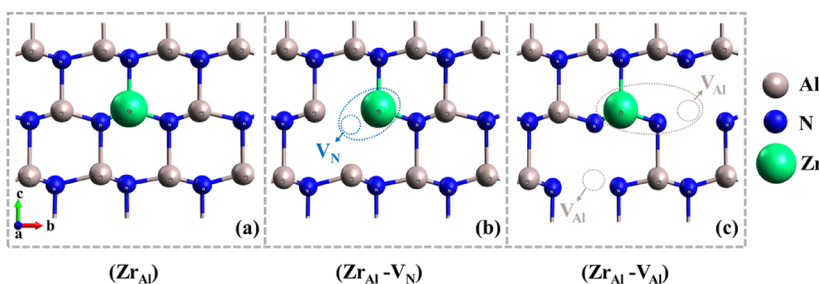
**FIG. 5.** Illustrations of optical processes involving the  $(\text{Zr}_{\text{Al}}-\text{V}_{\text{N}})$  complexes in AlN:Zr at room temperature ( $T = 300$  K). (a) Optical absorption and (b) optical emission. Emission lines related to  $(\text{V}_{\text{Al}})$  and  $(\text{V}_{\text{Al}}-\text{Complex})$  are also included. Allowed charge states of these defect complexes are indicated on the right side of the figure, whereas the charge states involved in the observed optical processes are shown on the left side of the transition lines. Possible spin conserving internal (intradefect) transitions in  $(\text{Zr}_{\text{Al}}-\text{V}_{\text{N}})^0$  are illustrated in enclosed red rectangles on the left. The transition lines observed in MOCVD grown AlN:Zr epilayers shown in Figs. 1, 2, and 4 are marked in black, theoretical predictions<sup>18</sup> are marked in red, and measurements obtained from Zr-implanted AlN<sup>19</sup> are marked in green.

Fig. 5(b) depicts the emission processes involving the  $(\text{Zr}_{\text{Al}}-\text{V}_{\text{N}})$  complexes. In Fig. 5, the optical transition lines observed in MOCVD grown AlN:Zr epilayers shown in Figs. 1, 2, and 4 are marked in black, theoretical predictions<sup>18</sup> are marked in red, and measurements obtained from Zr-implanted AlN<sup>19</sup> are marked in green. We would like to indicate that the observed energy levels for the same Zr-defect complex in the optical absorption and emission processes may not necessarily be the same because lattice relaxation or Stoke's shift is involved.<sup>18,23</sup>

In Fig. 5, allowed charge states of these defect complexes are indicated on the right side of the figure, whereas the charge states involved in the observed optical processes are shown on the left side of the transition lines. Possible spin conserving internal (intradefect) transitions in  $(\text{Zr}_{\text{Al}}-\text{V}_{\text{N}})^0$  are illustrated in enclosed red rectangles on the left. Emission lines related to  $(\text{V}_{\text{Al}})$  and  $(\text{V}_{\text{Al}}-\text{Complex})$  observed in undoped AlN and AlN:Zr are also included. Our results indicate that the most dominant optical absorption and emission processes in AlN:Zr involve  $(\text{Zr}_{\text{Al}}-\text{V}_{\text{N}})^0$ , which is highly

encouraging because  $(\text{Zr}_{\text{Al}}-\text{V}_{\text{N}})^0$  is predicted to be an ideal candidate of qubit. Understanding its related defect levels and corresponding energy transitions is critical for tailoring the properties of  $(\text{Zr}_{\text{Al}})$  defects and defect complexes in AlN for potential application as single-spin centers and solid-state qubits.

On the other hand, the presence of these defect complexes affects the structure, optical, and electrical properties of AlN. Figure 6 illustrates possible effects of Zr doping on the microscopic structures of AlN: (a) Zr substitutes onto the Al site (large solid green circles), forming a simple donor. This simple donor has an energy level around 1.4 eV,<sup>18</sup> although it is not clearly resolved in the optical absorption spectrum shown in Fig. 1(a). (b) Due to a much larger atomic size of Zr than Al, Zr doping can cause one of the nearest neighbors of  $\text{Zr}_{\text{Al}}$  to be missing and a  $(\text{Zr}_{\text{Al}}-\text{V}_{\text{N}})$  defect complex to be generated. The observed PL spectra shown in Figs. 2 and 4 indicate that  $(\text{Zr}_{\text{Al}}-\text{V}_{\text{N}})$  complexes are easily incorporated and are the dominant impurities exhibiting emission peaks at 3.63 and 2.46 eV. (c) In AlN:Zr, when Zr atoms substitute onto the Al sites, the Fermi level tends to shift toward the CBM, reducing the



**FIG. 6.** Illustration of possible atomic configurations of AlN:Zr, including impurities, vacancies, and complexes: (a) Zr substituting onto an Al site to form a donor, (b) Zr substitution accompanied with a generation of a neighboring  $\text{V}_{\text{N}}$ , and (c) Zr substitution accompanied with a generation of  $\text{V}_{\text{Al}}$ . The view is along the (0001) crystallographic plane.

formation energies of  $V_{Al}$  and its complexes and thereby generating more ( $V_{Al}$ ) defect complexes, which is confirmed by the observation of the much-enhanced emission intensity at 3.45 eV associated with the ( $V_{Al}$ -complex). The presence of defect complexes could influence local strain, charge compensation, and defect-related optical transitions. Analogous to the successful control of  $n$ -type conductivity in Si-doped AlN, the concentration of  $V_{Al}$ -complexes in AlN:Zr materials can be minimized by optimizing growth conditions, including the use of a low V/III ratio, a pulsed growth scheme, and a low growth rate.<sup>26–29</sup> Our results indicate that the formation of ( $Zr_{Al}$ - $V_N$ ) complexes is a dominant process in the growth of AlN:Zr, which makes AlN:Zr epitaxial materials highly promising for applications in quantum technologies.

In addition, the deep level nature of  $Zr_{Al}$  simple donors and ( $Zr_{Al}$ - $V_N$ ) complexes ( $\sim 1.4$  and  $\sim 1.8$  eV, respectively), together with AlN's high critical field, makes a strong case for utilizing AlN:Zr as a material for extrinsic photoconductive semiconductor switches (PCSS). The energy levels of  $Zr_{Al}$  and ( $Zr_{Al}$ - $V_N$ ) are sufficiently deep to facilitate an extremely low leakage current. A significant advantage of extrinsic PCSS over intrinsic PCSS is their capacity to support a large optical absorption length. This characteristic allows for the conduction throughout the bulk of the devices, thereby enabling high-voltage and high-power operation. While research on AlN:Zr epilayers is in a very early stage, understanding the optical properties of these impurities and defect complexes is critical for potential applications.

In summary, AlN:Zr epitaxial layers have been synthesized by MOCVD, and their optical properties have been investigated using absorption and PL spectroscopy. Distinct optical transitions, not present in undoped AlN, were identified in the AlN:Zr layers. These experimental results, together with calculations, allowed the construction of an energy level diagram for optical processes involving Zr-related complexes, confirming that Zr doping strongly modifies AlN's optical behavior. The impact of Zr doping contrasts sharply with that of Si doping. While Si introduces shallow ( $Si_{Al}$ ) donors for  $n$ -type conductivity, often compromised by ionization effects impacting compensation and mobility, Zr primarily forms deep-level, optically active neutral defects of ( $Zr_{Al}$ )<sup>0</sup> and ( $Zr_{Al}$ - $V_N$ )<sup>0</sup>. Their neutrality preserves carrier mobility, making Zr doping advantageous for applications leveraging these specific defect properties, such as quantum information, piezoelectric devices, and photoconductive switches. A remaining challenge, however, is that Zr doping also appears to promote the formation of undesirable  $V_{Al}$ -related centers. Suppression of these detrimental defects during synthesis is crucial for optimizing AlN:Zr device performance.

The information, data, or work presented herein was funded in part by the Advanced Research Projects Agency-Energy (ARPA-E), U.S. Department of Energy, under the ULTRAFast program, Award No. DE-AR0001821, monitored by Dr. Olga Spahn, Dr. Johan Enslin, and Dr. Eric Carlson. The views and opinions of the authors expressed herein do not necessarily state or reflect those of the United States Government or any agency thereof. Jiang and Lin are grateful to the AT & T Foundation for the support of the Ed Whitacre and Linda Whitacre endowed chairs.

## AUTHOR DECLARATIONS

### Conflict of Interest

The authors have no conflicts to disclose.

### Author Contributions

**H. Alwan:** Data curation (equal); Formal analysis (equal); Investigation (equal); Methodology (equal); Software (equal); Validation (equal); Visualization (equal); Writing – original draft (equal). **M. Almohammad:** Data curation (equal); Formal analysis (equal); Investigation (equal); Methodology (equal); Software (equal); Validation (equal); Visualization (equal). **J. Li:** Data curation (equal); Formal analysis (equal); Investigation (equal); Methodology (equal); Project administration (equal); Resources (equal); Software (equal); Supervision (equal); Validation (equal); Visualization (equal). **J. Y. Lin:** Conceptualization (equal); Formal analysis (equal); Funding acquisition (equal); Investigation (equal); Methodology (equal); Project administration (equal); Resources (equal); Supervision (equal); Validation (equal); Visualization (equal); Writing – review & editing (equal). **H. X. Jiang:** Conceptualization (equal); Formal analysis (equal); Funding acquisition (equal); Investigation (equal); Methodology (equal); Project administration (equal); Resources (equal); Supervision (equal); Validation (equal); Visualization (equal); Writing – review & editing (equal).

### DATA AVAILABILITY

The data that support the findings of this study are available within the article.

### REFERENCES

- J. Li, K. B. Nam, M. L. Nakarmi, J. Y. Lin, H. X. Jiang, P. Carrier, and Su-H. Wei, "Band structure and fundamental optical transitions in wurtzite AlN," *Appl. Phys. Lett.* **83**, 5163 (2003).
- K. B. Nam, J. Li, M. L. Nakarmi, J. Y. Lin, and H. X. Jiang, "Unique optical properties of AlGaN alloys and related ultraviolet emitters," *Appl. Phys. Lett.* **84**, 5264 (2004).
- Y. Taniyasu, M. Kasu, and T. Makimoto, "An aluminium nitride light-emitting diode with a wavelength of 210 nanometres," *Nature* **441**, 325 (2006).
- A. Khan, K. Balakrishnan, and T. Katona, "Ultraviolet light-emitting diodes based on group three nitrides," *Nat. Photonics* **2**, 77 (2008).
- Z. Zhang, M. Kushimoto, T. Sakai, N. Sugiyama, L. J. Schowalter, C. Sasaoka, and H. Amano, "A 271.8 nm deep-ultraviolet laser diode for room temperature operation," *Appl. Phys. Express* **12**, 124003 (2019).
- Q. Wang, S. Zhao, A. T. Connie, I. Shih, Z. Mi, T. Gonzalez, M. P. Andrews, X. Z. Du, J. Y. Lin, and H. X. Jiang, "Optical properties of strain-free AlN nanowires grown by molecular beam epitaxy on Si substrates," *Appl. Phys. Lett.* **104**, 223107 (2014).
- T. L. Chu and R. W. Kelm, "The preparation and properties of aluminum nitride films," *J. Electrochem. Soc.* **122**, 995 (1975).
- G. A. Slack, "Nonmetallic crystals with high thermal conductivity," *J. Phys. Chem. Solids* **34**, 321 (1973).
- R. L. Xu, M. M. Rojo, S. M. Islam, A. Sood, B. Vareskic, A. Katre, N. Mingo, K. E. Goodson, H. G. Xing, D. Jena, and E. Pop, "Thermal conductivity of crystalline AlN and the influence of atomic-scale defects," *J. Appl. Phys.* **14**, 126 (2019).

- <sup>10</sup>Z. Cheng, Y. R. Koh, A. Mamun *et al.*, “Experimental observation of high intrinsic thermal conductivity of AlN,” *Phys. Rev. Mater.* **4**, 044602 (2020).
- <sup>11</sup>P. Bagheri, C. Quiñones-García, D. Khachariya, S. Rathkanthiwar, P. Reddy, R. Kirste, S. Mita, J. Tweedie, R. Collazo, and Z. Sitar, “High electron mobility in AlN:Si by point and extended defect management,” *J. Appl. Phys.* **14**, 185703 (2022).
- <sup>12</sup>S. Strite and H. Morkoç, “GaN, AlN, and InN: A review,” *J. Vac. Sci. Technol., B* **10**, 1237 (1992).
- <sup>13</sup>*Properties of Advanced Semiconductor Materials: GaN, AlN, InN, BN, SiC, SiGe*, edited by M. E. Levinstein, S. L. Rumyantsev, and M. S. Shur (John Wiley & Sons, 2001).
- <sup>14</sup>M. A. Khan, A. Bhattarai, J. N. Kuznia, and D. T. Olson, “High electron mobility transistor based on GaN-Al<sub>x</sub>Ga<sub>1-x</sub>N heterojunction,” *Appl. Phys. Lett.* **63**, 1214 (1993).
- <sup>15</sup>Y. H. Chen, J. Encomendero, C. Savant, V. Protasenko, H. G. Xing, and D. Jena, “Electron mobility enhancement by electric field engineering of AlN/GaN/AlN quantum-well HEMTs on single-crystal AlN substrates,” *Appl. Phys. Lett.* **124**, 152111 (2024).
- <sup>16</sup>M. Hiroki, Y. Taniyasu, and K. Kumakura, “High-temperature performance of AlN MESFETs with epitaxially grown n-type AlN channel layers,” *IEEE Electron Device Lett.* **43**, 350 (2022).
- <sup>17</sup>T. Kumabe, A. Yoshikawa, S. Kawasaki, M. Kushimoto, Y. Honda, M. Arai, J. Suda, and H. Amano, “Demonstration of AlGaN-on-AlN p-n diodes with dopant-free distributed polarization doping,” *IEEE Trans. Electron Devices* **71**, 3396 (2024).
- <sup>18</sup>J. B. Varley, A. Janotti, and C. G. Van de Walle, “Defects in AlN as candidates for solid-state qubits,” *Phys. Rev. B* **93**, 161201(R) (2016).
- <sup>19</sup>A. Aghdaei, R. Pandiyan, B. Ilahi, M. Chicoine, M. El Gowini, F. Schiettekatte, L. G. Fréchette, and D. Morris, “Engineering visible light emitting point defects in Zr-implanted polycrystalline AlN films,” *J. Appl. Phys.* **128**, 245701 (2020).
- <sup>20</sup>A. Senichev, Z. O. Martin, Y. Wang, O. M. Matthiessen, A. Lagutchev, H. Htoon, A. Boltasheva, and V. M. Shalaev, “Quantum emitters in aluminum nitride induced by heavy ion irradiation,” *APL Quantum* **1**, 036103 (2024).
- <sup>21</sup>T. Yokoyama, Y. Iwazaki, Y. Onda, T. Nishihara, Y. Sasajima, and M. Ueda, “Effect of Mg and Zr co-doping on piezoelectric AlN thin films for bulk acoustic wave resonators,” *IEEE Trans. Ultrason. Ferroelectrics Freq. Control* **61**, 1322 (2014).
- <sup>22</sup>H. Alwan, N. K. Hossain, J. Li, J. Y. Lin, and H. X. Jiang, “Growth and characterization of high-quality Zr doped AlN epilayers,” *Appl. Phys. Lett.* **126**, 022106 (2025).
- <sup>23</sup>Q. Yan, A. Janotti, M. Scheffler, and C. G. Van de Walle, “Origins of optical absorption and emission lines in AlN,” *Appl. Phys. Lett.* **105**, 111104 (2014).
- <sup>24</sup>K. B. Nam, M. L. Nakarmi, J. Y. Lin, and H. X. Jiang, “Deep impurity transitions involving cation vacancies and complexes in AlGaN alloys,” *Appl. Phys. Lett.* **86**, 222108 (2005).
- <sup>25</sup>N. Nepal, M. L. Nakarmi, J. Y. Lin, and H. X. Jiang, “Photoluminescence studies of impurity transitions in AlGaN alloys,” *Appl. Phys. Lett.* **89**, 092107 (2006).
- <sup>26</sup>M. L. Nakarmi, K. H. Kim, K. Zhu, J. Y. Lin, and H. X. Jiang, “Transport properties of highly conductive n-type Al-rich Al<sub>x</sub>Ga<sub>1-x</sub>N ( $x \geq 0.7$ ),” *Appl. Phys. Lett.* **85**, 3769 (2004).
- <sup>27</sup>P. F. Mehnke, T. Wernicke, M. Kneissl, and F. Tuomisto, “Electrical compensation and cation vacancies in Al-rich Si doped AlGaN,” *Appl. Phys. Lett.* **117**(14), 142103 (2020).
- <sup>28</sup>M. H. Breckenridge, P. Bagheri, Q. Guo, B. Sarkar, D. Khachariya, S. Pavlidis, J. Tweedie, R. Kirste, S. Mita, P. Reddy, R. Collazo, and Z. Sitar, “High *n*-type conductivity and carrier concentration in Si-implanted homoepitaxial AlN,” *Appl. Phys. Lett.* **118**, 112104 (2021).
- <sup>29</sup>T. Jamil, A. A. M. Mazumder, M. Rahman, M. Ali, J. Lin, H. Jiang, G. Simin, and A. Khan, “Si-doped AlN using pulsed metalorganic chemical vapor deposition and doping,” *Appl. Phys. Express* **18**, 025501 (2025).
- <sup>30</sup>L. Bergman, M. Dutta, C. Balkas, R. F. Davis, J. A. Christman, D. Alexson, and R. J. Nemanich, “Raman analysis of the E1 and A1 quasi-longitudinal optical and quasi-transverse optical modes in wurtzite AlN,” *J. Appl. Phys.* **85**, 3535 (1999).